Effect of Filamentation of Brillouin Scattering in Large Underdense Plasmas Irradiated by Incoherent Laser Light [Phys. Rev. Lett. 75, 4413 (1995)]

T. Afshar-rad, L. A. Gizzi, M. Dessleberger, and O. Willi

We regret that in the printed version of the manuscript, Figs. 2(a)–2(c) were interchanged with Figs. 3(a)–3(c). In addition, the published Fig. 3(d) was incorrect. As the principal conclusion of the article was based upon a comparison of Figs. 2(a) and 2(b) to Figs. 3(a) and 3(b), this error may have prevented many readers from comprehending the Letter. We are therefore reprinting it correctly below.

 0031-9007/96/76(17)/3242(5)$06.00

Effect of Filamentation of Brillouin Scattering in Large Underdense Plasmas Irradiated by Incoherent Laser Light

T. Afshar-rad, L. A. Gizzi, M. Desselberger, and O. Willi

The Blackett Laboratory, Imperial College of Science and Technology, Prince Consort Road, London SW7 2BZ, United Kingdom

(Received 25 January 1995; revised manuscript received 5 June 1995)

An experimental study of stimulated Brillouin backscatter (B-SBS), produced in a large "homogeneous" underdense plasma using induced spatially incoherent laser light, is presented. The observations reveal that a strong correlation exists between the level of B-SBS and laser filamentation. It is suggested that a filamentory model of B-SBS is needed to better describe the scattering process under conditions of high laser irradiance and large plasma scale lengths.

PACS numbers: 52.40.Nk, 52.25.Rv, 52.35.Nx, 52.50.Lp

The study of parametric instabilities, generated in a plasma by an intense electromagnetic pulse, is of both fundamental and practical importance [1]. In inertial confinement fusion (ICF), for example, the occurrence of such instabilities has long been recognized as being detrimental to the success of direct-drive laser fusion schemes. One such instability, namely, stimulated Brillouin scattering (SBS), has been at the center of much investigation in recent years [1,2]. A key goal for researchers has been to improve the ability to predict and control the growth of this instability under conditions relevant to ICF. Progress has been made in this area, with recent studies suggesting that the "smoothing" of high powered laser beams using the induced spatial incoherence (ISI) technique can be effective in suppressing SBS growth [2]. However, although these results are very encouraging, some fundamental questions still need to be addressed. Interactions with higher irradiances, and larger plasma scale lengths, are required to establish whether ISI can maintain its effectiveness. Also, there still remain major discrepancies between observations and theoretical predictions, and as yet a clear understanding of the causes of instability suppression has not emerged. A possible means of clarifying some of these discrepancies is to gauge the role that other instabilities play in regulating SBS. Most significantly, the role played by the filamentation instability needs to be assessed since evidence for the occurrence of strong filamentation activity has already been demonstrated in large scale-length plasmas for coherent laser light [3]. In this Letter we present an experimental study of stimulated Brillouin backscatter (B-SBS), produced in a large "homogeneous" underdense plasma column by an intense laser pulse, over nearly 2 orders of magnitude in irradiance (10^{13}–10^{15} W cm^{-2}). The laser-plasma interaction was studied at both green ($\lambda_0 = 0.53$ μm) and infrared ($\lambda_0 = 1.06$ μm) laser wavelengths using temporally and spatially incoherent laser light. Spatial incoherence was achieved using the induced spatial incoherence technique [4]. The evidence indicates that the formation of laser filaments controls the onset of B-SBS emission and supports a correlation between the suppression of B-SBS and the effectiveness of ISI in suppressing filamentation.

For the experiment present here, the underdense plasma column was generated by exploding a thin aluminum foil target (0.3 mm wide, 0.5 mm long, 700 nm thick) using two opposing pairs of laser beams [laser wavelength $\lambda_0 = 0.53$ μm, full width at half maximum (FWHM) $\cong$ 600 ps] [3,5,6]. The total heating irradiance was approximately 10^{14} W cm^{-2}. An interaction laser beam, delayed by $t_D = 1.7$ ns with respect to the end of the heating pulse, was then focused into the plasma column along its longitudinal axis using a 1 m aspheric lens ($f/10$ optics). In the far field of the lens the measured FWHM focal diameter was around 120 μm. At $t_D = 1.7$ ns, the electron density and temperature were measured to be $N_e \cong 3.2 \times 10^{20}$ cm^3 and $T_e \cong 500$ eV using uv interferometry and time-resolved x-ray spectroscopy, respectively [6]. The absence of a critical density surface at the time of interaction, and the uniform plasma density and temperature along the propagation length, allowed a "modeled" study of the interaction process to be made. The B-SBS was collected using the $f/10$ focusing lens and relayed onto a fast calibrated photodiode to measure the level of backscatter. For the green laser, the spatial profile of the transmitted interaction beam was recorded by imaging the exit plane of the plasma column onto the slit of an S20 streak camera or onto a 2D framing camera (120 ps gate time). The spatial profile of the B-SBS was recorded by imaging the interaction region onto the slit of an S20 streak camera. The spatial and temporal resolution of the imaging system was calculated to be 5 μm and 10 ps, respectively, with the measured values $\cong$ 1.5 times greater.

Laser-plasma interactions were investigated at both infrared ($\lambda_0 = 1.06$ μm) and green ($\lambda_0 = 0.53$ μm) laser wavelengths using either (i) a normal coherent laser, (ii) a broadband laser only (without ISI echelons), or (iii) a broadband laser with ISI echelons included. The ISI was generated using a broadband oscillator ($\Delta\omega/\omega \cong 0.1\%$, laser coherence time $t_c = 1/\Delta\nu = 2$ ps for $\lambda_0 = 0.53$ μm) and a 6×6 echelon array to produce 36 independent beamlets. The ISI laser (FWHM $\cong$ 700 ps $\pm$ 15%) has a rise time of $\cong$ 100 ps and a near flattop temporal profile. A more detailed description of the ISI

 0031-9007/96/76(17)/3242(5)$10.00

system is given elsewhere [4,6]. Figure 1 shows the measured B-SBS fraction ($E_{SBS}\%$) as a function of the average irradiance I ($W\,cm^{-2}$). With the infrared broadband laser we observe a B-SBS "threshold" occurring at $I \cong 2 \times 10^{13}\,W\,cm^{-2}$ and a "saturation" level of $E_{SBS} \cong 4\%$. A similar saturation level was also recorded with the infrared coherent laser. This is to be expected, since the condition required for the laser bandwidth to moderate B-SBS is not valid here; i.e., $\gamma_0/\Delta\omega \ll 1$, where γ_0 is the B-SBS homogeneous growth rate [7]. The B-SBS fraction for the green coherent interaction is also included in Fig. 1 for comparison, outlined by the shaded region. With the infrared ISI, the backscatter was reduced to $E_{SBS} \cong 10^{-2}\%$ at $I \cong 3 \times 10^{13}\,W\,cm^{-2}$, but grew with increasing irradiance to $E_{SBS} \cong 0.5\%$ for $I \cong 8 \times 10^{14}\,W\,cm^{-2}$. By comparison, the B-SBS fraction with green ISI did not exceed the dipole detection level. However, it was estimated using the spatial and spectral diagnostics to be $E_{SBS} \cong 10^{-3}\%$, well below the non-ISI level at $E_{SBS} \cong 1\%$.

In Figs. 2(a)–2(c) we present a typical data set obtained with the green-coherent laser interaction beam. This has been included to "bridge the gap" between coherent and ISI-laser interactions, and help in our understanding and interpretation of the data presented for the ISI interactions. Figure 2(a) and 2(b) are two 1D spatially resolved streaks of the B-SBS emission at $I = 10^{15}\,W\,cm^{-2}$ and $I = 5 \times 10^{14}\,W\,cm^{-2}$, respectively. These clearly show that the emission emanates predominantly from localized regions. Both transitory ($\leq$20 ps) and more prolonged bursts of emission ($\leq$300 ps) can be identified, with typical transverse scale lengths $\leq 10\ \mu m$. For the coherent laser interactions direct evidence for the occurrence of strong filamentation activity has already been established by us under similar interaction conditions, and will not be discussed in detail here; see Coe, Afshar-rad, and Willi in Ref. [3]. In Ref. [3] evidence for filamentation was established by comparing the level of intensity modulations (I_{max}:I_{av}) present in the transmitted beam profile with that of the incident beam, for which I_{max}:$I_{av} \cong 2:1$. This enabled a direct evaluation to be made of any intensity "enhancement" at the exit plane. Significant intensity enhancement, and a corresponding reduction in the diameter of the intensity channels formed, gave clear evidence of strong filamentation activity. Further, a "lower-bound" intensity value of $8 \times 10^{13}\,W\,cm^{-2}$ was experimentally established, below which no evidence for "enhanced" breakup was detected [3]. This was found to be in reasonable agreement with the onset of filamentation activity. Here, the presence of laser filamentation was established as before. Principally, by analyzing the spatial profile of the transmitted laser beam for evidence of enhanced intensity channeling, after its propagation through the preformed plasma column. In Fig. 2(c) we present a typical 1D spatially resolved streak of the transmitted beam recorded at $I = 6 \times 10^{14}\,W\,cm^{-2}$, showing significant enhanced beam breakup. Corresponding 2D spatial images of the transmitted beam profile obtained with a framing camera reveal intensity modulations I_{max}:$I_{av} > 7:1$, well above those of the incident beam (see also Ref. [3]). Following the theoretical treatment of filamentation theory given in Ref. [8] (see Table I in Ref. [8]), we would expect that both thermal (TF) and ponderomotive (PF) forces contribute to the initial self-focusing of the incident "hotspots." Then, as the filament radius shrinks, the ponderomotive forces should rapidly dominate the process

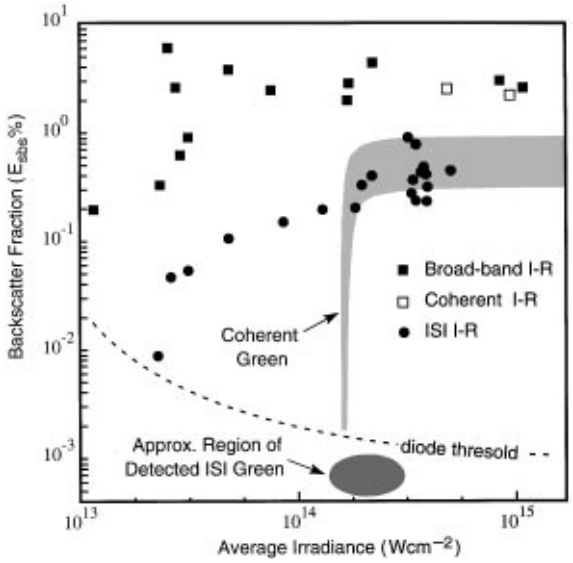

FIG. 1. The B-SBS energy fraction ($E_{SBS}\%$) as a function of the time-averaged interaction irradiance I ($W\,cm^{-2}$) for infrared and green laser interactions.

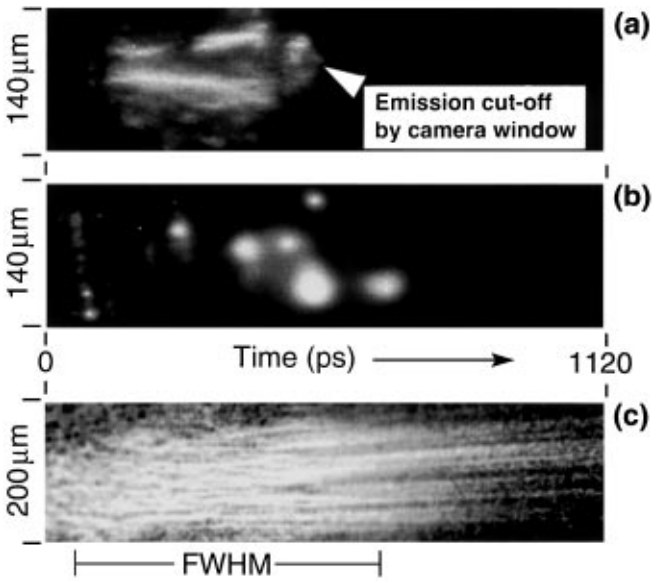

FIG. 2. (a)–(c) A typical spatial profile data set with green-coherent interaction. (a) and (b) are two 1D spatially resolved streaks of the B-SBS emission at $I = 10^{15}\,W\,cm^{-2}$ and $I = 5 \times 10^{14}\,W\,cm^{-2}$, respectively. These clearly reveal the emission emanating from localized regions. (c) is a 1D spatially resolved streak of the transmitted beam recorded at $I = 6 \times 10^{14}\,W\,cm^{-2}$, showing enhanced breakup of the beam.

[3]. However, recent theoretical developments by Epperlein and Short suggest that nonlocal heat transport may play a key role in the filamentation process [9]. It is suggested that a reduction in the effective thermal conductivity relative to its classical value, due to nonlocal transport, will enhance the TF growth rate and make it the dominant mechanism. The degree to which kinetic effects actually contribute to filament formation here could not be experimentally assessed. However, the optimum growth lengths predicted by Epperlein and Short [see Eq. (18) in Ref. [9]], suggest that filamentation formation should occur for irradiances as low as 3×10^{12} W cm^{-2} for our conditions. This is approximately an order of magnitude lower than the optimum growth rate predicted for "conventional" ponderomotive filamentation, and is well below the lower-bound irradiance level for which breakup was actually observed [3]. In order to assess the theoretical feasibility of filament formation for our conditions we shall adopt a classical approach and consider only the PF component, since the inclusion of the TF component can only enhance the filamentation process. For the incident hot spots scale lengths measured ($\lambda_\perp = 24$–14 μm), the PF intensity threshold is predicted to occur at $I_T \cong (0.6$–$2) \times 10^{14}$ W cm^{-2} for $\lambda = 0.53$ μm. For $\lambda = 1.06$ μm, the threshold $I_T \cong (1$–$4) \times 10^{13}$ W cm^{-2} [8].

Figures 3(a)–3(d) show a corresponding spatial data set recorded with green-ISI laser interactions. Figure 3(a) shows a typical B-SBS spatially resolved streak image with a time-averaged irradiance of 4.5×10^{14} W cm^{-2}. The emission exhibits localized bursts that produce a "spotty" emission profile similar to that observed with the coherent laser interactions at moderate intensities. This emission is too coarse, both temporally and spatially, to attribute it to the instantaneous ISI intensity fluctuations occurring at the focus. We would expect these nonuniformities to shift randomly on a time scale of the laser coherence time $t_c \cong 2$ ps (for $\lambda = 0.53$ μm). The resulting B-SBS emission would "wash out" any emission structure since $t_c \ll$ temporal resolution. To establish the origins of these localized bursts of emission we examine the spatial profile of the transmitted laser beam as above. Figure 3(b) is the corresponding 1D spatially resolved streak of the transmitted ISI beam for Fig. 3(a). Clearly, when contrasted with the coherent laser interaction there is a noticeable reduction in the breakup of the transmitted beam. However, more careful analysis shows that the ISI beam profile still exhibits some regions of intensity enhancement. These enhanced regions are of short duration, typically between 10 and 100 ps. This can clearly be seen in Fig. 3(c), which shows a 2D intensity map of Fig. 3(b). For the sake of clarity in the presentation, the base-level intensity in Fig. 3(c) has been set at 1.5 times the averaged spatial intensity ($1.5I_{\rm av}$). This effectively eliminates ISI "noise," arising from the expected level of ISI fluctuations, and only those regions where a clear enhancement has occurred are shown. From Fig. 3(c) we can see that spatial intensity peaks of $I_{\rm max}/I_{\rm av} \geq 3$ are present, with the most intense region having saturated. Figure 3(d) shows a typical gated 2D spatial image of the transmitted ISI beam (gate time = 120 ps, taken at $t = 600$ ps), recorded

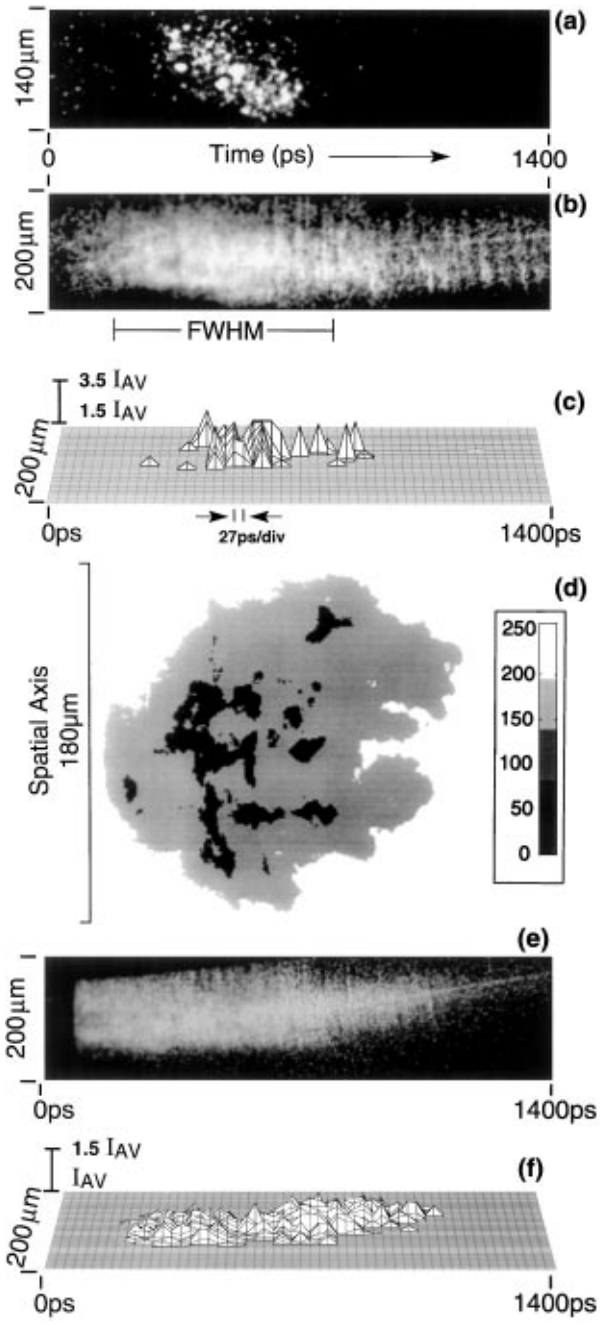

FIG. 3. (a)–(f) A typical data set recorded with green-ISI interaction. (a) shows a B-SBS spatially resolved streak at $I = 4.5 \times 10^{14}$ W cm^{-2}, exhibiting localized bursts of emission. (b) is the corresponding 1D spatially resolved streak of the transmitted ISI beam that still exhibits some regions of intensity enhancement. (c) shows a 2D intensity plot of (b). (d) is a typical 2D spatial image of the transmitted ISI beam (120 ps camera gate time), presented as a three-level intensity contour map, revealing the spatial distribution of the intensity enhanced regions. In (e) a 1D spatial streak of the transmitted ISI beam at the "lower-bound" irradiance of $\cong 7.5 \times 10^{13}$ W cm^{-2} is presented. (f) is the corresponding 2D intensity mapping of (e).

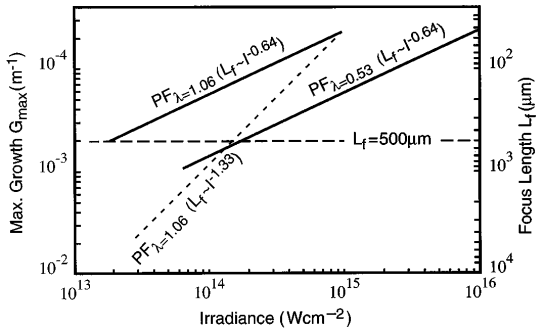

FIG. 4. The PF maximum spatial growth rates $G_{\max}$ (m^{-1}) and focusing lengths L_f (μm) versus interaction intensity for the infrared and green ISI (solid lines) predicted by simulation. Also included for comparison (dashed line) is the analytical model prediction for infrared; see Fig. 17 in Ref. [8].

at the same laser irradiance. The image is presented as a three-level intensity contour map, which clearly demonstrates the spatial distribution of the enhanced regions. These were found to persist in the transmitted profile despite attempts to optimize the focusing conditions at these higher irradiances. As with the coherent interactions, a lower-bound intensity value was established for which no evidence of breakup could be detected in the beam profile after its propagation through the plasma column. In Fig. 3(e) a 1D spatial streak of the transmitted ISI beam at the lower-bound irradiance of $\cong 7.5 \times 10^{13}\ \mathrm{W\,cm^{-2}}$ is presented. Figure 3(f) is the corresponding 2D intensity mapping made of Fig. 3(e). In contrast with Fig. 3(b) no evidence for intensity enhancement can be observed. Further, no B-SBS emission was recorded in any of the diagnostic channels below an irradiance of $\cong 10^{14}\ \mathrm{W\,cm^{-2}}$; see also Fig. 1. The intensity fluctuations that are recorded in Fig. 3(f) do not exceed $1.3I_{\mathrm{av}}$, and are consistent with the natural background pattern expected with an ISI beam over short time cycles. Line scans made of Fig. 3(e) show that the laser intensity has a root-mean-square deviation $\sigma_{\mathrm{rms}} \cong 0.13 \pm 0.2$. This is, in fact, lower, by a factor of 2.5 times, than the predicted ISI rms deviation for the incident ISI beam that follows a $(t_c/t)^{1/2}$ dependence [10]. Here we taken t to be temporal resolution of 15 ps. This would suggest that, in the absence of filamentation, the plasma itself can act to smooth the background ISI fluctuations. This may possibly be attributed to small-scale scattering caused by plasma density perturbations [3,8].

On the basis of these observations it could reasonably be concluded that the transitory nature of the enhanced intensity regions observed is consistent with the formation of quasi-steady-state filaments as predicted in 2D (and 3D) simulations presented by Schmitt [8]. To justify this statement the strength of ISI-laser filamentation needs to be gauged. We shall again consider the effect of the ponderomotive mechanism, although as already explained above we do not rule out the possibility that he TF mechanism is also a component in the filamentation process, particularly in the early stages of filament formation. The maximum PF growth rates ($G_{\max}$) and focusing lengths ($L_f \cong 1/G_{\max}$) are plotted in Fig. 4, as a function of laser irradiance. The dashed line represents an analytical calculation using the quasi-steady-state filamentation model (see Table II in Ref. [8]). However, 2D (and 3D) simulations performed by Schmitt show that the analytical model provides only a moderately accurate treatment of the PF mechanism [8]. This occurs because the degree of smoothing assumed in the analytical model is overestimated for the smaller scale length PF modes. The PF local position derived from simulations suggests the scaling $L_f \sim I^{-0.64}$ (solid lines), as opposed to $L_f \sim I^{-1.33}$ (dashed line). For infrared ISI at $I \geq 10^{15}\ \mathrm{W\,cm^{-2}}$ the analytical and simulation values for L_f are assumed to coincide since $\lambda_{\perp\,\max}^{\mathrm{PF}} <$ minimum incident perturbation $\lambda_{\perp\,\min} = 10\lambda_0$ with $F\#10$ optics, see Fig. 17 in Ref. [8]. For green ISI, $\lambda_{\max}^{\mathrm{PF}} < \lambda_{\perp\,\min}$ when $I_0 \geq 10^{16}\ \mathrm{W\,cm^{-2}}$. The scaling for L_f confirms that filamentation activity can occur within our plasma column (length $= 500\ \mu$m). With infrared ISI, the expected onset of B-SBS at $I \cong 3 \times 10^{13}\ \mathrm{W\,cm^{-2}}$ appears to be in reasonable agreement with the onset of filamentation. With green ISI this should occur at $I \cong 10^{14}\,\mathrm{W\,cm^{-2}}$, as confirmed by the SBS spectral and spatial diagnostic.

In summary, measurements of B-SBS with and without ISI echelons are presented that clearly reveal the strong correlation between the level of B-SBS and the inferred strength of laser filamentation. With ISI, operated at moderate irradiances, filamentation activity is certainly reduced. However, the residual B-SBS observed still originates from regions where quasi-steady-state filaments have formed. Increasing the irradiance naturally results in increasing filamentation and thus in raising the B-SBS level. In the limit, as the effectiveness of ISI to suppress filamentation breaks down, the B-SBS approaches levels comparable with the coherent laser interactions. The results suggest that the role of laser beam filamentation needs to be considered in any detailed description of the B-SBS.

The authors acknowledge the support of the Rutherford Appleton Laboratory. This work was partially funded by EPSRC/MoD grants.

[1] W. L. Kruer, Comments Plasma Phys. Controlled Fusion **6**, 167 (1981).
[2] A. N. Mostovych *et al.*, Phys. Rev. Lett. **59**, 1193 (1987); S. E. Coe *et al.*, Europhys. Lett. **10**, 31 (1989).
[3] S. E. Coe, T. Afshar-rad, and O. Willi, Opt. Commun. **46**, 299 (1989); O. Willi *et al.*, Phys. Fluids B **2**, 1318 (1990).
[4] C. N. Danson *et al.*, Annual Report to the Laser Facility, Report No. RAL-89–043, 1989; R. H. Lehmberg and S. P. Obenschain, Opt. Commun. **46**, 27 (1983).
[5] R. A. London and M. Rosen, Phys. Fluids **29**, 3813 (1986).
[6] T. Afshar-rad, PhD. thesis, University of London, (1992).
[7] J. J. Thompson, Nucl. Fusion **15**, 237 (1975).
[8] A. J. Schmitt, Phys. Fluids **31**, 3079 (1988); Phys. Fluids B **3**, 186 (1991).
[9] E. M. Epperlein and R. W. Short, Phys. Fluids B **4**, 2211 (1992).
[10] S. Skupsky *et al.*, J. Appl. Phys. **66**, 3456 (1989).